Seismic detection of a spatially-limited fluid pulse ascending a growth fault: Modeling and interpretation

Matthew Haney[1], Roel Snieder[1], and Jon Sheiman[2]
[1] *Center for Wave Phenomena, Colorado School of Mines, Golden, CO 80401*
[2] *Shell International Exploration and Production Inc., Houston, TX 77025*

ABSTRACT

We report on what is, to our knowledge, the first image of a fluid pulse inside a fault-zone that, based on geochemical evidence, is ascending the fault with time. The fluid pulse is confined to a growth fault (the B-fault) at the South Eugene Island 330 field, offshore Louisiana. Though the thickness of the fault-zone may only be tens of meters, or a fraction of a seismic wavelength, at the location of the fluid pulse, it is detectable because the fluid pulse is of high fluid pressure and, hence, low P-wave velocity. We extract the amplitude of the fault-plane reflection from the B-fault by applying a dip-filter to migrated 3D seismic data gathered by Shell in 1992. The reflectivity at the location of the fluid pulse is roughly three times greater than at an unremarkable part of the B-fault where a sonic log passed through the fault in 1993. We modify the sonic log by placing a 30 m low velocity zone at the fault-plane, representing a model of the fluid pulse. After generating synthetic seismograms from both the sonic log and the modified sonic log, we find that the low velocity zone produces high reflectivity similar to that observed at the fluid pulse. The ability to detect such a spatially-limited, high fluid pressure anomaly has implications for the understanding of hydrocarbon migration mechanisms and the time scale of reservoir-recharge in the Gulf of Mexico.

Key words: episodic fluid flow, faults, hydrocarbon migration

Introduction

Faults have long been characterized as zones of highly focused deformation and fluid flow in the subsurface; the exact mechanism of fluid flow and rate of flow along faults are, however, not well understood. For instance, Revil and Cathles (2002) claim that fluids may propagate as solitary waves along faults at the rate of kilometers per year. Since faults deform, or slip, in an episodic manner, it has been postulated that flow along faults should also be episodic and linked to the slip events (Sibson, 1990). Episodic flow along faults may be common in sedimentary basins worldwide. In the Gulf of Mexico, growth faults cutting through young, poorly consolidated sediments provide a means for hydrocarbons generated in deep source rocks to migrate into shallower, economically producible reservoirs.

We have previously established from 3D seismic data collected at the South Eugene Island field, offshore Louisiana, that fault-plane reflections from the main basin-bounding growth fault (the A-fault) indicate the portions over which the fault acts as a lateral seal (Haney *et al.*, 2004). In this brief paper, we extend our interpretation of the seismic data to examine the possibility that the faults at South Eugene Island also act as vertical conduits for fluid migration. Such behavior has been observed during the Global Basins Research Network (GBRN) drilling project at South Eugene Island (Anderson *et al.*, 1995) and highlights the dual nature of faults as both effective lateral seals and vertical fluid migration pathways.

We find that at one location, the intersection of the A10ST well with a fault synthetic to the A-fault, known as the B-fault, high fault-plane reflectivity occurs where a fluid pulse has been documented from drilling records

(Losh *et al.*, 1999). Using a sonic log that passes through part of the B-fault, we perform some simple numerical modeling to estimate the dimensions and properties of a fluid pulse confined to the fault-zone. We conclude that a thin, low velocity zone, consistent with the presence of a fluid pulse, could be responsible for the high reflectivity at the B-fault. Due to the zone being only a fraction of a seismic wavelength, a trade-off exists between the elastic properties of the pulse, its thickness, and the magnitude of its reflection. As a result, more than one model of a low velocity zone gives an identical reflection.

Vertical fluid migration at South Eugene Island

The South Eugene Island field displays strong evidence of vertical fluid migration from deep source rocks into its shallow Plio-Pleistocene reservoirs (Revil and Cathles, 2002). This phenomenon has been given the name dynamic fluid injection. Evidence of recent and fast fluid migration up the growth faults comes from the present day oil seeps at the fault scarps on the sea floor (Anderson *et al.*, 1995), the variation in the chemistry of petroleum fluids over the time scale of years (Whelan *et al.*, 2001), and geochemical anomalies observed near the A-fault in the A6ST well (Losh *et al.*, 1999).

Extensive drilling and geologic studies have taken place at South Eugene Island. The best known is the multifaceted GBRN DOE-funded drilling project that took place in the mid-1990's. During late 1993, GBRN intentionally drilled into and successfully cored several of the growth faults at South Eugene Island. The wells GBRN drilled into the A-fault and B-fault began in the downthrown, hydrostatically pressured sediments and passed through the faults into overpressured (upthrown) sediments. At most of the wells, the B-fault was found to be overpressured relative to the downthrown sediments, but not more overpressured than the upthrown block; the one exception was at the A10ST well. As participants in the GBRN drilling project, Losh *et al.* (1999) concluded that "except for the A10ST well, the fault itself does not generally represent a zone of low effective stress (high fluid pressure) relative to the upthrown sediments, but it is at significantly lower vertical effective stress than downthrown sediments." Furthermore, Losh *et al.* (1999) claimed that "the isolated pocket of anomalously high fluid pressure in the A10ST well may represent a spatially limited pulse of anomalously pressured fluid." Recently, Losh and Cathles (2004) identified the pulse at A10ST as an ascending fluid pulse initiated by episodic slip on the fault. With this information, we decided to apply our dip-filtering technique for studying fault-plane reflections (Haney *et al.*, 2004) to the B-fault, especially near the A10ST well.

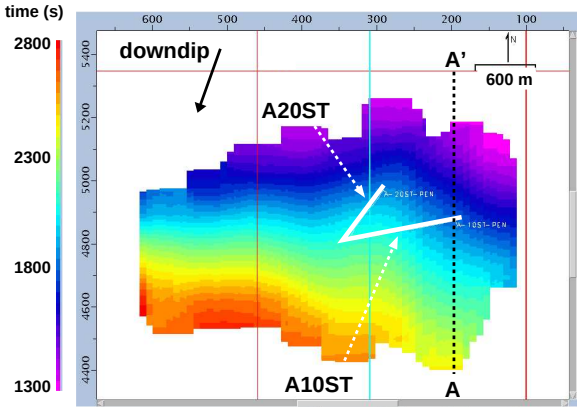

Figure 1. Map view of the two-way reflection time from the B-fault. The fault dips toward the southwest, as indicated by the arrow in the upper left portion of the plot. The line A-A′ is shown in the N-S direction and the paths of two wells, the A10ST and the A20ST, are shown projected onto the horizontal plane.

Locally high reflectivity at the A10ST well

Our processing sequence for interpreting fault-plane reflections begins by manually picking the fault-plane of interest in a time-migrated 3D seismic data volume. In Fig. 1, we show a time-map of the B-fault from our picks. We then dip-filter the seismic data in the direction of fault dip to accentuate the fault-plane reflections while simultaneously attenuating the reflections from the flat layers. The final step is to extract the maximum amplitude of the fault-plane reflection, which lies close to our picked fault-plane. We select the maximum amplitude within a time gate of 100 ms around our picked fault-plane.

In Fig. 2, we show an overlay of the seismic data along the A-A′ line (see Fig. 1) with its dip-filtered version. From this image, one can see the fault-plane reflections that occur over portions of the A-fault and the B-fault. These fault-plane reflections, as discussed in Haney *et al.* (2004), are due in large part to a sharp increase in pore pressure across parts of the A-fault and B-fault. The sharp increase in pore pressure results in an equally sharp decrease in seismic velocity, as shown in Fig. 3 by a velocity/pore-pressure relationship we constructed from wells at South Eugene Island. As the pore pressure increases, the differential stress (the difference between the lithostatic stress and the pore pressure) plotted in Fig. 3 decreases. Since most of the overpressure at South Eugene Island is caused by undercompaction, the decrease in the differential stress is correlated with a decrease in seismic velocity. Losh *et al.* (1999) have documented a decrease of differential pressure by 800 psi over a distance of 18 m while drilling into

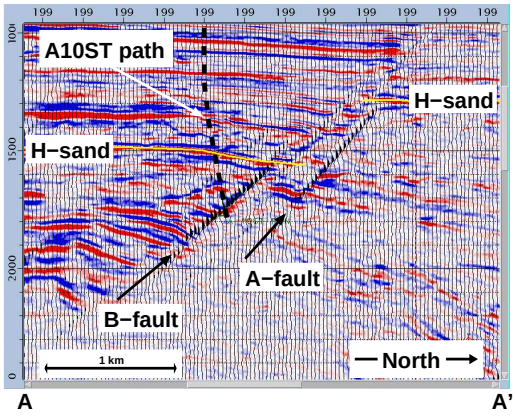

Figure 2. Overlay of the time-migrated seismic data (variable density) with a dip-filtered version (wiggle trace) of the same data along line A-A′. The dip-filtering is in the direction of fault dip to accentuate fault-plane reflections. The H-sand is highlighted to indicate the total throw across the A-fault and B-fault. The path of the A10ST well is projected into the A-A′ plane. The vertical axis is two-way-time in milliseconds and, taking the approximation that 1 ms two-way-time = 1 m depth, the vertical exaggeration of the plot is about 2×.

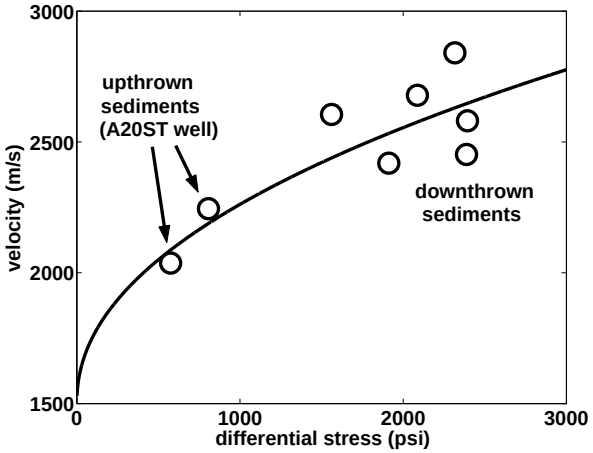

Figure 3. A plot of sonic velocity versus differential stress compiled from wells where both a fluid pressure measurement and a sonic log existed. Data points are shown as circles. The pressure data used to construct the plot comes from Losh *et al.* (1999) and the velocity data comes from sonic logs available at Shell. Data from both the upthrown and downthrown sediments have been included in this plot, with the measurements from the upthrown sediments coming exclusively from the A20ST well. The six data points from the downthrown sediments each represent a different well. The sonic velocity is seen to decrease as the differential stress decreases, or equivalently, as the fluid pressure rises. Also shown is a best-fit Bowers type relation as a solid line (Sayers *et al.*, 2003).

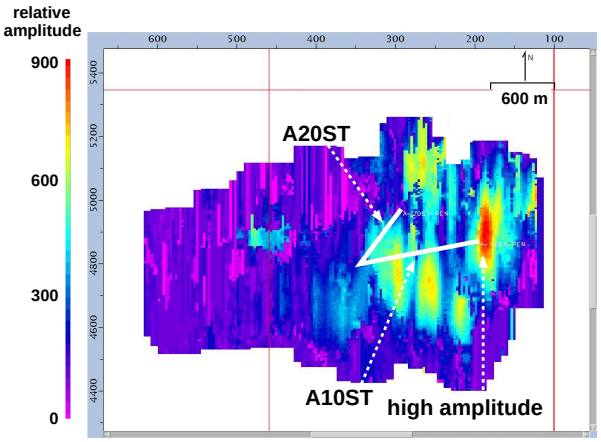

Figure 4. Reflection amplitude from the B-fault as a function of position on the fault-plane. The view is the same as in Fig. 1. Note the smearing of the reflection amplitudes in the up-down direction due to the dip-filter processing we employed to isolate the fault-plane reflection from the B-fault. The A20ST well, which intersected the B-fault in a "dead-zone", does not encounter an unusually high-amplitude anomaly on the fault-plane. In contrast, the A10ST well, which encountered a fluid pulse at the B-fault, terminates into the strongest reflecting portion of the fault. The reflectivity at the intersection of the A10ST well is approximately three times greater than at the A20ST well.

the A-fault. Other factors that are not plotted in Fig. 3, such as porosity and lithology, may also play a role in defining the overpressures at South Eugene Island.

After extracting the maximum amplitude of the fault-plane reflection from the B-fault, we obtain the reflectivity map shown in Fig. 4. Strong reflectivity, shown as brighter colors, come and go on the fault-plane due to the sharp lateral sealing of the B-fault. However, the strongest reflection amplitude occurs at the intersection of the A10ST well with the B-fault - where a fluid pulse has been reported by Losh *et al.* (1999). At this location, we hypothesize that the fault-plane reflection arises due to a combination of the sharp lateral seal and the spatially-limited fluid pulse in the fault zone. We test this hypothesis in the next section by constructing synthetic seismograms with a sonic log from the A20ST well that crosses the B-fault. Finally, we note that, from the reflectivity map in Fig. 4, the magnitude of the fault-plane reflection at the A10ST well is three times larger than the reflection at the A20ST well, where we have sonic velocity information.

Numerical modeling from A20ST sonic log

To better understand the variation of elastic properties that could give rise to the high reflectivity ob-

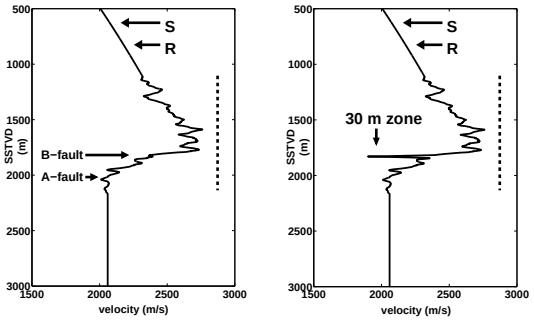

Figure 5. The two models of velocity as a function of depth that we used in our synthetic seismograms. On the left is the model for the A20ST well and, on the right, the model for the A10ST well. For the A20ST well, we use its smoothed sonic log for the velocity over a depth range of about 1 km, marked by a vertical dashed line. Above this depth range, we allow the velocity to smoothly decrease according to the compaction trend of Fig. 3. We keep the velocity constant below the depth range of the sonic log. Note the sharp decrease in velocity at around 1800 m due to the B-fault acting as a pressure seal at the A20ST well. The model for the A10ST well is the same as for the A20ST well, except that we insert a 30 m zone with a velocity of 1900 m/s. The depths of the source and receiver for the seismograms in Fig. 6 are displayed at the tops of the models.

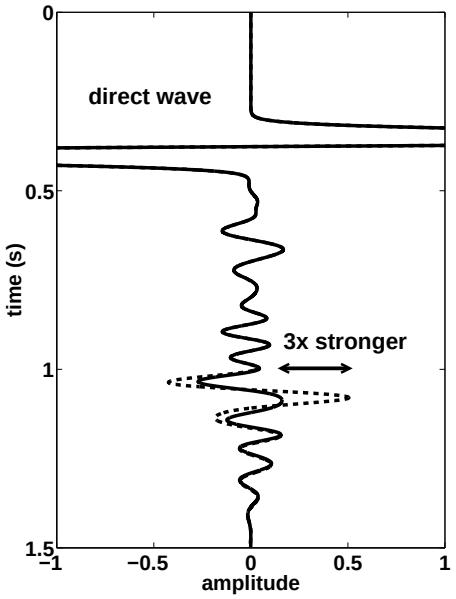

Figure 6. The synthetic seismograms for the A20ST (solid) and A10ST (dashed) models. Since the only difference in the two models is the 30 m low-velocity zone, the seismograms are identical until 1 s. At that point, the low-velocity zone in the A10ST model produces a reflection approximately three times stronger than the reflection due to only the sharp decrease in velocity at the B-fault in the A20ST model. This factor corresponds to the relative difference in the reflectivity observed between the intersections of the A20ST and A10ST wells in Fig. 4.

served at the A10ST well, we generated synthetic seismograms from a sonic log. Unfortunately, no sonic log existed for the A10ST well; however, a sonic log was acquired through the B-fault at the nearby A20ST well. A smoothed version of this sonic log is shown in left panel of Fig. 5. Note that, since the fault zone at the A20ST well was not overpressured relative to the upthrown sediments, the only imprint of the B-fault on the sonic log is the sharp velocity decrease due to the B-fault acting as a lateral seal in this location.

We use the sonic log from A20ST as the physical basis for our numerical modeling. First, we simulate the reflection from the fault-plane due to the sharp decrease in velocity that occurs at the A20ST well. We utilize a finite-element implementation of the wave equation with a normally incident P-wave source of 10 Hz dominant frequency. Hence, we do not consider conversions to S-waves. Furthermore, we assume constant density since the sonic log shows substantially more variation than the density log. Secondly, we simulate the reflection from the same sharp velocity decrease, except we add a 30 m zone of anomalously low velocity (see the right plot of Fig. 5) at the B-fault. This model is consistent with the dimensions of the fault zone described by Losh *et al.* (1999) and the degree of additional overpressure in the fluid pulse (Losh, 2004; personal communication). Since we smoothed the sonic log at a length scale of 1/10 the dominant seismic wavelength, the low velocity zone is also tapered over its thickness, reaching its lowest velocity of 1900 m/s at its center.

The synthetic seismograms are plotted in Fig. 6. The main waveforms are the direct wave, the reflections from the sedimentary layers, and the reflection from the B-fault. For both models, the seismograms are identical until the reflection from the B-fault arrives. The maximum amplitude of the fault-plane reflection from the A10ST model, which includes a low velocity zone, is approximately three times larger than the associated fault-plane reflection from the A20ST sonic log. The model qualitatively agrees with the relative strengths of fault-plane reflections at A10ST and A20ST observed on the reflectivity map of Fig. 4. Though the above model of a low velocity zone qualitatively matches our observations, we note that a 15 m zone with a velocity of 1500 m/s produces exactly the same reflection as the 30 m zone with a velocity of 1900 m/s.

Conclusion

We have observed anomalously high reflectivity associated with a portion of a growth fault in the Gulf of Mexico where others have speculated, based on drilling records and geochemical evidence, that a fluid pulse is ascending the fault. By generating synthetic seismograms based on a sonic log that passes through the

fault, we have demonstrated that a low velocity zone at the fault-plane qualitatively agrees with the relative strength of reflected amplitudes in seismic data. The ability of reflected seismic waves to detect a fluid pulse could lead to a better understanding of hydrocarbon migration or an entirely new play concept based on drilling hydrocarbons in a fault zone. Future work will attempt to observe the fluid pulse move in different vintages of seismic data taken over a period of ten years. Other possible causes of the amplitude anomaly at A10ST, in addition to stacking errors and AVO effects, will also be explored.

Acknowledgments

The authors thank Steven Losh of Cornell for access to the A20ST well logs and for numerous discussions about South Eugene Island. Shell International Exploration and Production has provided funding for this research.

REFERENCES

Anderson, R. N., Billeaud, L. B., Flemings, P. B., Losh, S., and Whelan, J. K. 1995. *Results of the Pathfinder Drilling Program into a Major Growth Fault, Part of the GBRN/DOE Dynamic Enhanced Recovery Project in Eugene Island 330 Field, Gulf of Mexico*, Global Basins Research Network, Lamont-Doherty Earth Observatory.

Haney, M., Sheiman, J., Snieder, R., Naruk, S., Busch, J., and Wilkins, S. 2004. Fault-plane reflections as a diagnostic of pressure differences in reservoirs: South Eugene Island, offshore Louisiana, in: *Proceedings of EAGE Special Session on Fault and Top Seals*, Montpellier, France.

Losh, S., Eglinton, L., Schoell, M., and Wood, J. 1999. Vertical and Lateral Fluid Flow Related to a Large Growth Fault, South Eugene Island Block 330 Field, Offshore Louisiana. *AAPG Bulletin*, **83**, *244-276.*

Losh, S. and Cathles III, L. 2004. Fault Conduit/Fault Seal Behavior, South Eugene Island Block 330 Field, Offshore Louisiana, in: *Proceedings of EAGE Special Session on Fault and Top Seals*, Montpellier, France.

Revil, A. and Cathles III, L. M. 2002. Fluid transport by solitary waves along growing faults: A field example from the South Eugene Island Basin, Gulf of Mexico. *Earth and Planetary Science Letters*, **202**, *321-335.*

Sayers, C. M., Smit, T. J. H., van Eden, C., Wervelman, R., Bachmann, B., Fitts, T., Bingham, J., Mclachlan, K., Hooyman, P., Noeth, S., and Mandhiri, D. 2003. Use of reflection tomography to predict pore pressure in overpressured reservoir sands, 73rd Ann. Internat. Mtg. Soc. Expl. Geophys., Expanded Abstracts, 1362-1365.

Sibson, R. H. 1990. Conditions for fault-valve behavior, in: *Deformation Mechanisms, Rheology and Tectonics*, eds. R. J. Knipe and E. H. Rutter, Geological Society Special Publication No. 54, Alden Press, Oxford, 15-28.

Whelan, J. K., Eglinton, L., Kennicutt II, M. C., and Qian, Y. 2001. Short-time-scale (year) variations of petroleum fluids from the U. S. Gulf Coast, em Geochim. Cosmochim. Acta, **65**, *3529-3555.*